# FY21 Progress Report on BISON Simulation Development for ALD Coated Particles

**Chemical and Fuel Cycle Technologies Division**

**About Argonne National Laboratory**
Argonne is a U.S. Department of Energy laboratory managed by UChicago Argonne, LLC
under contract DE-AC02-06CH11357. The Laboratory's main facility is outside Chicago, at
9700 South Cass Avenue, Argonne, Illinois 60439. For information about Argonne
and its pioneering science and technology programs, see www.anl.gov.

# FY21 Progress Report on BISON Simulation Development for ALD Coated Particles

prepared by
A. Oaks, Z. Mei, A. Yacout
Chemical and Fuel Cycle Technologies Division, Argonne National Laboratory

September 30, 2021

**Summary**


# FY21 Progress Report on BISON Simulation Development for ALD Coated Particles

Argonne has on ongoing effort to perform atomic layer deposition coatings on micron-scale fuel particles. Initial results showed cracking of the coating layer above a specific coating thickness, which motived the development of a BISON model for the coated particle system to help explain the behavior. This report describes the initial development of the BISON model, the materials models used, and the conditions used in the simulation. A 2D model has been developed, with sensitivity studies performed on several key parameters. Based on the 2D model results, and 3D model was also developed, with results from all calculations described. First principles calculations were also performed on the fuel/coating interface to help describe the observed behavior. Potential future activities are also described.

**TABLE OF CONTENTS**

# FY21 Progress Report on BISON Simulation Development for ALD Coated Particles

## 1    INTRODUCTION

Argonne National Laboratory (ANL) has an ongoing effort to perform atomic layer deposition (ALD) coatings of uranium-carbon-nitride ($UC_{1-x}N_x$) fuel kernels, and the initial coatings were performed with zirconium nitride (ZrN). After the production of these coated particles, it was observed that when the coating thickness was greater than 200 nanometers, the coating surface would crack after cooling (Figure 1), but with thicknesses below 200 nanometers, the coatings remained intact with no observable cracks. This was potentially due to a mismatch between UCN and ZrN thermal expansion, lattice mismatch, surface conditions, cooling conditions, or some other reason that remains to be identified. The goal of this work was to develop a BISON [1] model of the coated particle system that can accomodate complexity as the work proceeds and be used to explore different coating materials. The observed cracking behavior in the ZrN coating provides a comparison case for the initial model as it is developed, so the initial effort was focused on modeling and simulating the cooldown behavior and exploring potential parameter changes to reduce the chance of coating cracking based on changes observed in the coating stress. In this initial development, uranium-nitride (UN) fuel properties were used due to the availability of appropriate models. First principles calculations were also performed on the UN/ZrN coating interface to explore if the observed behavior could be due to poor adhesion at the interface.



|         |         |
|:-------:|:-------:|
|   (a)   |   (b)   |

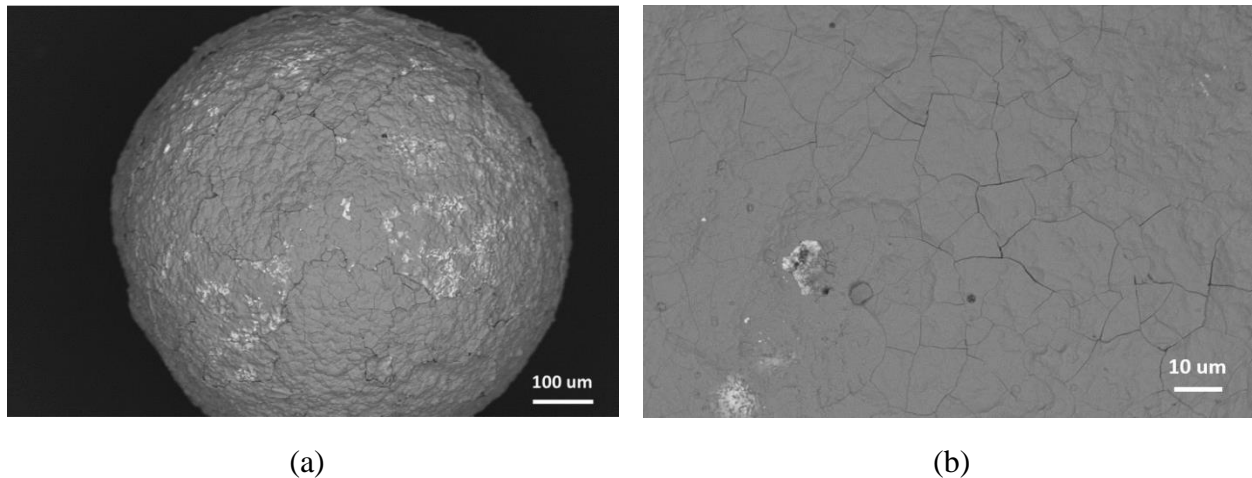Figure 1: Cracked ZrN coating on UCN fuel particle after ALD deposition and cooldown.

## 2    MATERIAL MODELS

This section covers the material models used in the BISON simulations for the UN fuel and ZrN coating. The BISON model collection had several preexisting UN material models available, but none for the ZrN coating. The needed models were found in literature and implemented in BISON using generic model interfaces.

## 2.1 UN Fuel

### 2.1.1 Thermal Conductivity

The UN thermal conductivity was available in the BISON model collection (UNThermal [2]) and was obtained from nitride fuel properties [3]. The thermal conductivity is given as a function of temperature and porosity:

$$k(T, p) = 1.37 \cdot T^{0.41} \frac{1 - p}{1 + p} \tag{1}$$

where $k$ is the thermal conductivity in W/m·K, $T$ is temperature in K, and $p$ is the kernel porosity.

### 2.1.2 Heat Capacity

The UN specific heat capacity was available in the BISON model collection (UNThermal [2]) and was obtained by fitting discrete UN heat capacities [4]. The specific heat capacity is given as a function of temperature:

$$C_p(T) = \frac{4.184}{M} \cdot \left( 12.1554383 + 0.0.00255593918\, T - \frac{544.292173}{T} + \frac{4359.06572}{T^2} \right) \tag{2}$$

where $C_p$ is the specific heat capacity in J/kg·K, $T$ is the temperature in K, and $M$ is the molar mass of the material.

### 2.1.3 Thermal Expansion

The UN thermal expansion was available in the BISON model collection (UNThermalExpansionEigenstrain [5]) and uses a correlation from NASAGRC (2019) [6]. The correlation depends on the material temperature, as well as the stress-free temperature. The stress-free temperature was taken to be the ALD reactor operating temperature.

### 2.1.4 Elastic Tensor

The UN elasticity tensor was available in the BISON model collection (UNElasticityTensor [7]) uses a correlation from NASAGRC (2019) [6] which depends on temperature and porosity.

### 2.1.5 Density

The UN density was implemented with the MOOSE Density model [8], and taken from [9] for room temperature (298 K):

$$\rho = 14.33 \tag{3}$$

where $\rho$ is the density in g/cm$^3$.

## 2.2 ZrN Coating

### 2.2.1 Thermal Conductivity

The ZrN thermal conductivity was implemented with the MOOSE HeatConductionMaterial model [10], and was taken to be constant [11]:

$$k = 20.5 \tag{4}$$

where $k$ is the thermal conductivity in W/m·K.

### 2.2.2 Heat Capacity

The ZrN heat capacity was implemented with the MOOSE HeatConductionMaterial model [10], and was taken to be a function of temperature [12]:

$$C_p(T) = 43.60 + 6.82 \times 10^{-3}T - 5.00 \times 10^5 T^{-2} \tag{5}$$

where $C_p$ is the heat capacity in J/K·mol, and $T$ is the temperature in K.

### 2.2.3 Linear Thermal Expansion

The ZrN thermal expansion was implemented with the MOOSE ComputeThermalExpansionEigenstrain model [13], with the thermal coefficient taken to be $\alpha = 7.24 \times 10^{-6}$ [14]:

$$\epsilon_{thermal}(T) = 7.24 \times 10^{-6} \left(T - T_{free}\right) \tag{6}$$

where $T$ is the temperature in K, and the $T_{free}$ is the stress-free temperature, taken to be the ALD reactor temperature.

### 2.2.4 Elastic Tensor

The ZrN elasticity tensor was implemented with the MOOSE ComputeIsotropicElasticityTensor model [15] with the Young's modulus and Poisson's ratio given by [11]:

$$E = 450 \, GPa \tag{7}$$
$$\nu = 0.25 \tag{8}$$

where $E$ is the Young's modulus and $\nu$ is the Poisson's ratio.

### 2.2.5 Density

The ZrN density was implemented with the MOOSE Density model [8], and taken from [16]:

$$\rho = 6500 \tag{9}$$

where $\rho$ is the density in kg/m$^3$.

## 3    2D MODEL DEVELOPMENT

The engineering scale modeling was performed using the BISON fuel performance code. The reference case was developed in 2D geometry, and was eventually extended into 3D, discussed in the next section.

### 3.1    Geometry

The 2D mesh was taken to be a concentric circular mesh, modeled as one quarter circle with symmetry conditions along the x-axis and y-axis, as shown in Figure 2. The mesh consists of two blocks, one for the UN fuel, and one for the ZrN coating. The fuel kernel was taken to be 800 microns in diameter, with the coating taken to be 100 nanometers thick. The mesh was generated internally in BISON using the MeshGenerator system, with greater resolution used in the coating region due to the relative difference in size.
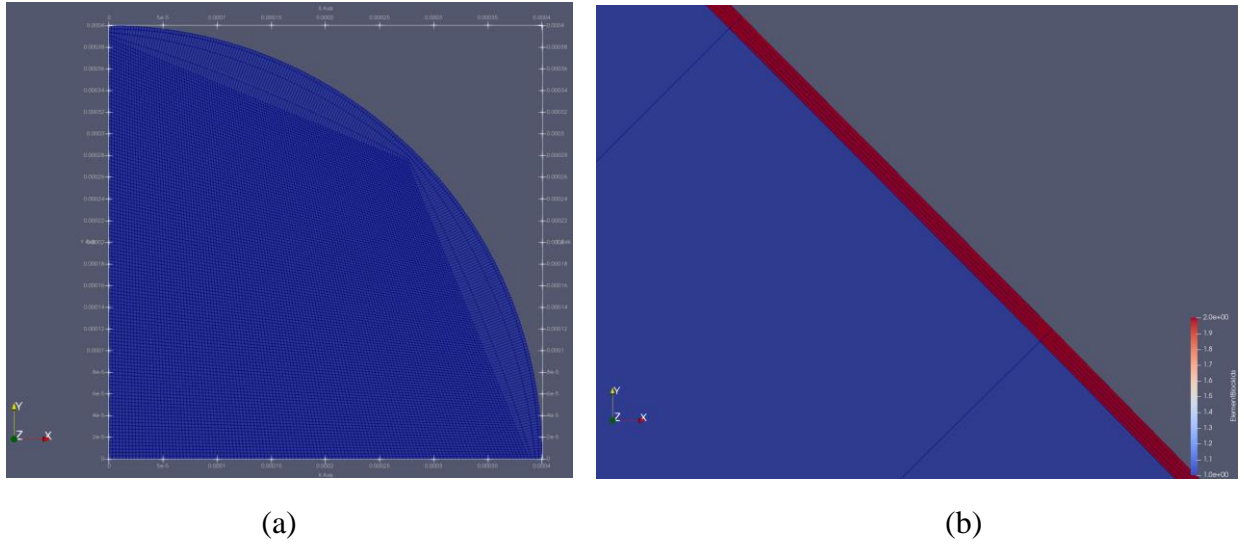


|         (a)          |         (b)          |

Figure 2: 2D concentric circle mesh with symmetry, (a) full size, (b) edge zoom to show coating.

### 3.2    Conditions

The exterior thermal boundary condition was chosen to simulate cooldown behavior of the coated fuel particles after the ALD coating process. The ALD reactor operating temperature is 240 $°C$, which was taken to be the initial condition for the entire mesh, and the outer surface was then specified to cool down to room temperature. This model used an approximation of the cooldown process, specifying the outer surface temperature directly to cooldown linearly from the reactor operating temperature to room temperature over the cooldown period, taken to be 1 hour in the reference case. Additional complexity could be added in future work to use a convective heat transfer boundary condition instead of specifying the temperature directly.

## 3.3    Reference Case

The primary objective of the work was to study the evolution of von Mises stress in the coating and study the effect of different parameters on this evolution. The reference case provides the basis for each of the parameter variations. In the reference case the coating von Mises stress steadily follows the boundary surface temperature condition. After reaching room temperature the maximum coating von Mises stress reaches approximately 107 MPa. These results are shown in Figure 3.
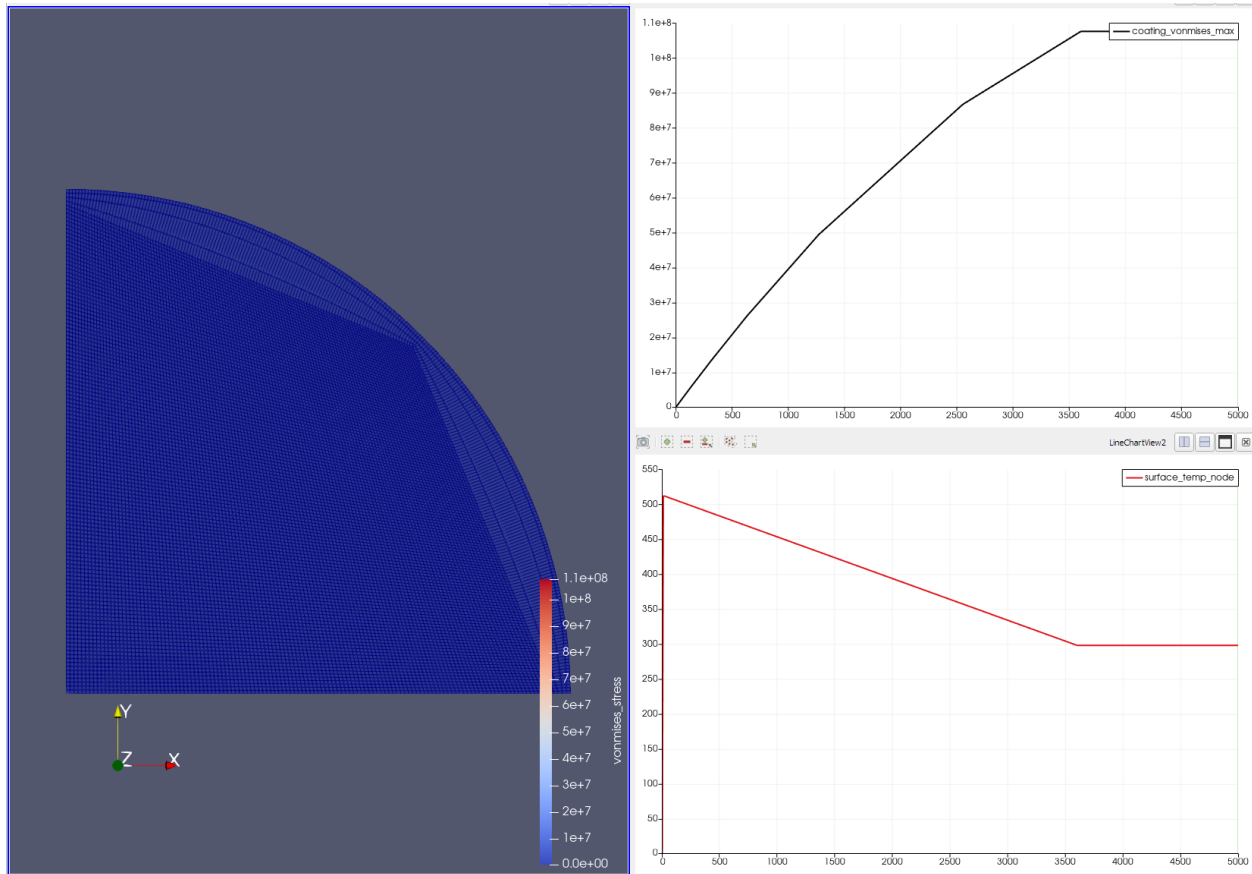


Figure 3: 2D reference case results. Surface temperature in K, peak coating von Mises stress in Pa.

## 3.4    Parameter Variation

With the reference case established in the previous section, several parameters were chosen to study the effect of variations on the coating stress: coating thickness, cooling time, fuel kernel size, and fuel kernel porosity. In each variation, the simulation was performed based on the reference case conditions, with only the specified parameter varied. For coating thickness, the thickness was varied from 100 nm up to 800 nm, which was expected to have a significant impact based on what had already been observed in fabrication results (Figure 4). For cooling time or cooling rate, the cooldown time was extended from 1 hour up to 6 hours (Figure 5). For kernel size, the radius was varied between 200 microns and 800 microns (Figure 6). Finally for kernel porosity, the porosity

was varied from 0 up to 30% (Figure 7). This is likely not a parameter that would want to be changed, but it was a parameter in some of the UN material properties, so it was still explored for reference.
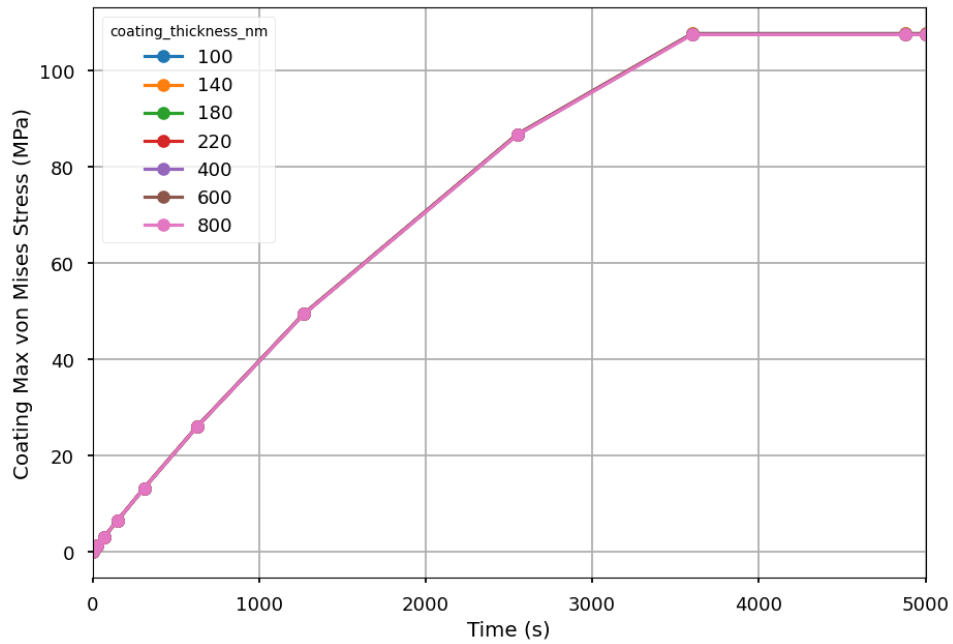


Figure 4: Coating peak von Mises stress results for coating thickness parameter sensitivity.
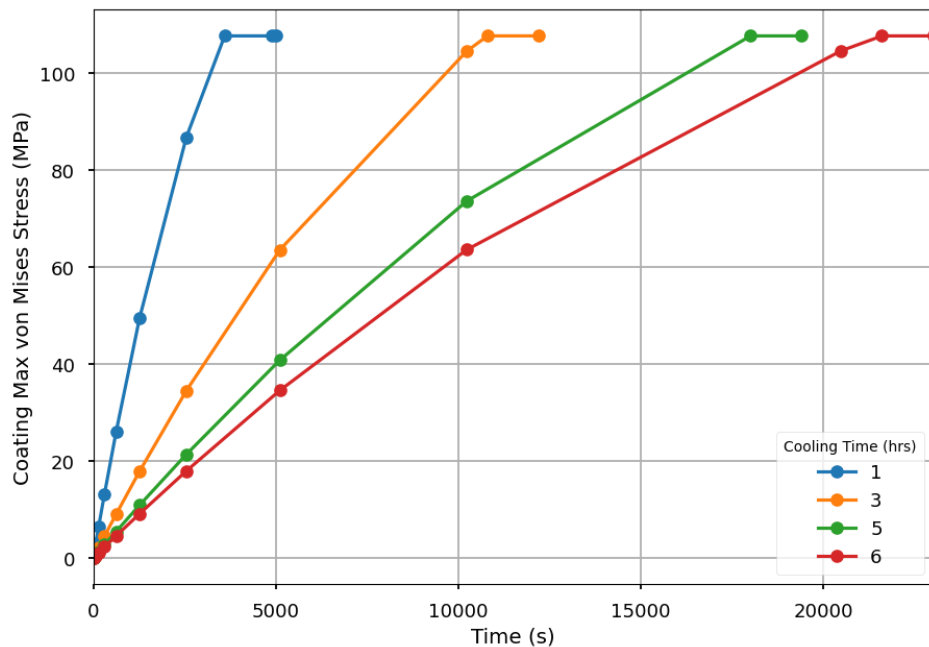


Figure 5: Coating peak von Mises stress results for cooling time parameter sensitivity.
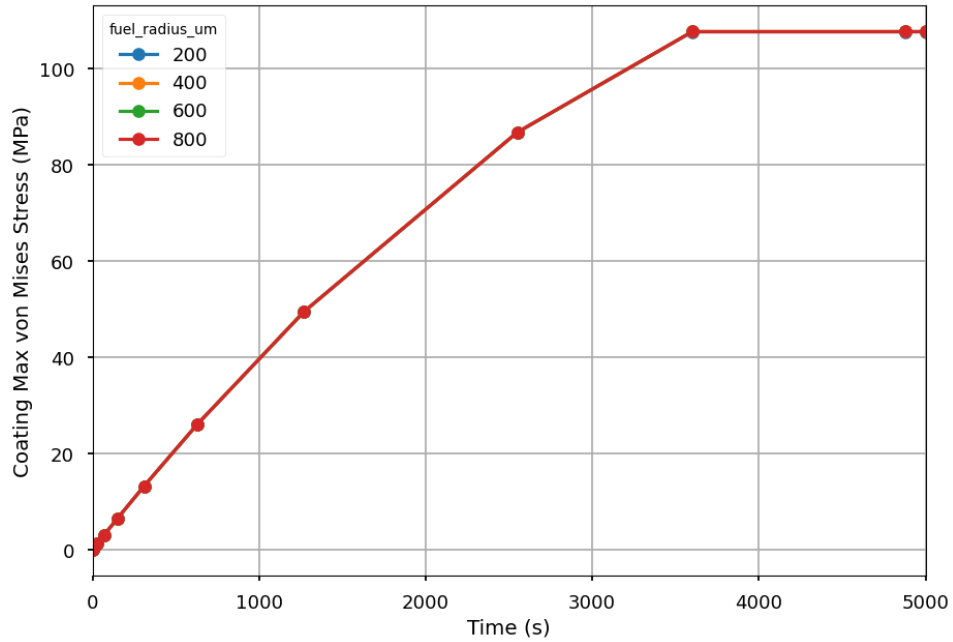
Figure 6: Coating peak von Mises stress results for fuel kernel radius parameter sensitivity.
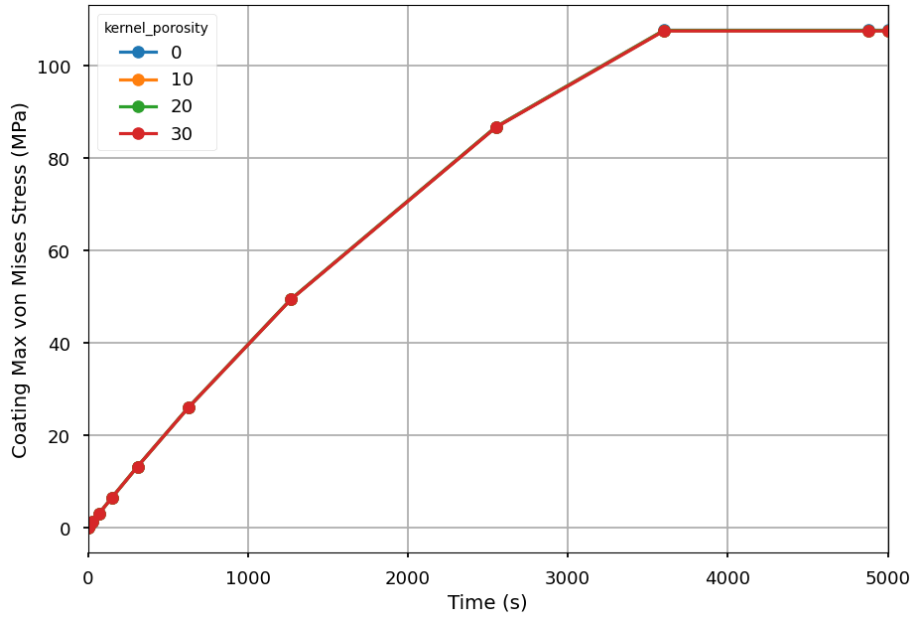


Figure 7: Coating peak von Mises stress results for fuel kernel porosity parameter sensitivity.

Despite initial predictions, the results showed that none of the variations resulted in any significant change in the coating stress. This was most surprising for variations in coating thickness, as differing behavior in the fabrication results had already been observed, and this indicated there were potentially missing key properties from the model. After further consideration it was thought that the cracking was potentially due to stress concentration due to the surface roughness of the

7

fuel kernel, which was not represented in the mesh, and that the basic 2D model would need to be extended to a 3D model with a rough surface to be able to capture the behavior that had observed experimentally.

## 4    3D MODEL DEVELOPMENT

This 3D BISON model expands on the 2D BISON model described in the previous section to account for a 3D mesh which includes surface defects.

### 4.1    Reference Case

The 2D quarter circle mesh was extended to a fully 3D spherical mesh. The conditions from the 2D reference case were then applied to the 3D mesh and same simulation was caried out. The resulting stress distribution is shown in Figure 8. The coating von Mises stress is symmetric about the spheric surface and reached a maximum of approximately 107 MPa. This is the same stress distribution as the 2D model, which provides some confidence that the 2D-to-3D transition was done correctly.
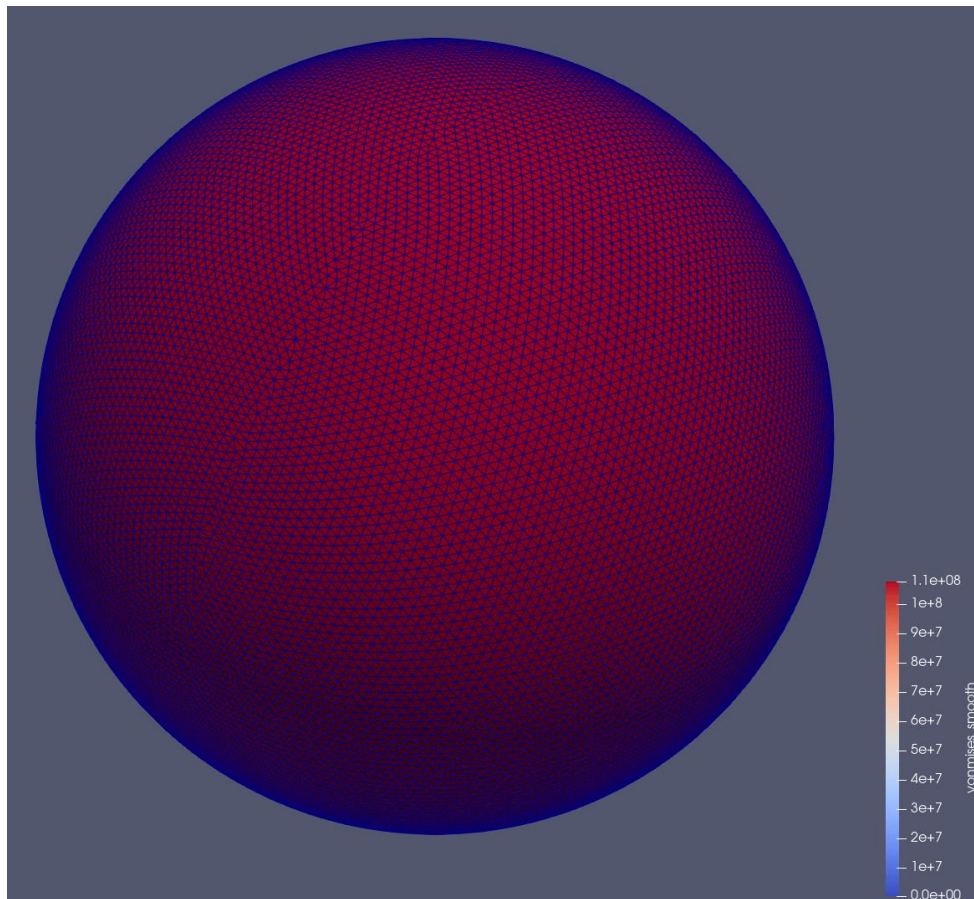


Figure 8: 3D smooth particle coating peak von Mises stress results.

## 4.2    Surface Defect Case

The smooth 3D sphere was then extended by creating a random assortment of surface defects. These defects don't precisely mimic the observed particle surface, but work as a reasonable first approximation. The same calculation was then performed on the defected mesh, with the results shown in Figure 9. The stress concentration is no longer uniform and concentrates around the surface defects, maxing out at around 375 MPa, roughly 3.5 times the original result. This indicates that the stress concentration is sensitive to the particle surface and provides confidence that the BISON model is progressing in the right direction.
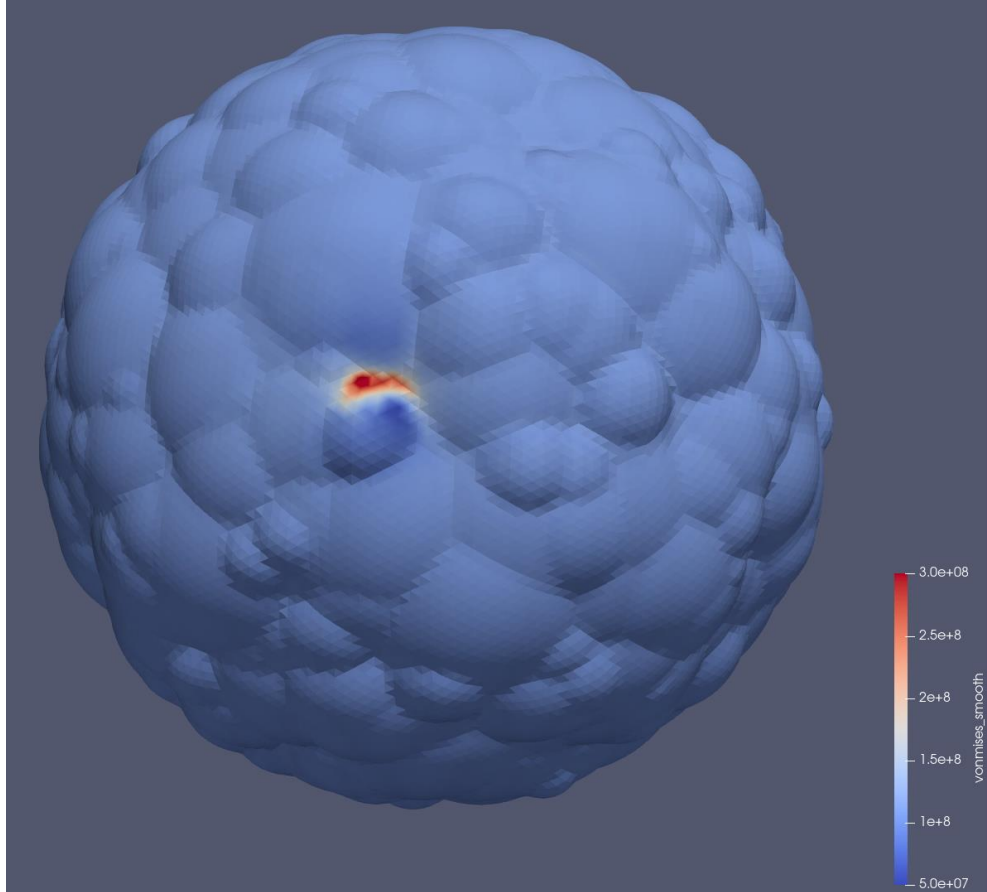


Figure 9: 3D defected particle coating peak von Mises stress results.

## 5    FIRST PRINCIPLES CALCULATIONS

To understand the adhesion behavior of ZrN coating on UN fuel and the potential role of $ZrO_2$ layer on the adhesion of ZrN coating on UN, density functional theory (DFT) calculations were performed to simulate the interfaces of UN/ZrN, UN/$ZrO_2$, and $ZrO_2$/ZrN. A previous study by Weinreich et al. [17] shows that the deposited $ZrO_2$ coating can be amorphous or crystalline phase (tetragonal/cubic) phase depending on the film thickness. For the $ZrO_2$ film deposited in this study, the $ZrO_2$ coating should be in crystalline phase, either tetragonal or cubic depends on the deposition conditions. For this reason, both tetragonal and cubic $ZrO_2$ were considered for generating the $ZrO_2$/ZrN interface. Crystalline ZrN and UN adopt the rock salt structure. Although the (100)

surface of ZrN is thermodynamically more stable than the (110) and (111) surfaces, the (111) surface orientation of ZrN is thermodynamically more favorable to form coherent interfaces with the (111) surface of tetragonal $ZrO_2$ (t-$ZrO_2$) because of the reduced lattice mismatch. To this end, a total of four interfaces were studied in this work: (1) UN(001)/ZrN(001), (2) UN(001)/c-$ZrO_2$(001) (both Zr and O terminations are considered for c-$ZrO_2$), (3) ZrN(001)/c-$ZrO_2$(001), and (4) ZrN(111)/t-$ZrO_2$(111). The generated interface structures are shown in Figure 10.

All DFT calculations were performed using the Vienna *ab initio* Simulation Package (VASP) [18, 19] based on the projector augmented wave method (PAW) [20]. The exchange-correlation functional is described by the Perdew-Burke-Ernzerhof (PBE) generalized gradient approximation (GGA) [21]. $6s^26p^65f^27s^2$, $4s^24p^65s^24d^2$, $2s^22p^3$, and $2s^22p^4$ electrons were treated as valence electrons for U, Zr, N and O atoms, respectively. A plane-wave kinetic-energy cutoff of 500 eV and a k-point sampling of $9\times 9 \times 1$ was used for all the interface calculations. The four interfaces, i.e., UN(001)/ZrN(001), UN(001)/c-$ZrO_2$(001), ZrN(001)/c-$ZrO_2$(001), and ZrN(111)/t-$ZrO_2$(111), were constructed using the optimized lattice parameters of the corresponding phases for UN, t-ZrN, c-ZrN and $ZrO_2$. Periodic slab models were used to simulate the interface structures. In these models, a finite number of layers of atoms were used to represent the semi-infinite bulk phase, and these slabs were separated by a region of vacuum thick enough to minimize the inter-slab interactions. The positions of all atoms in the slabs were fully relaxed before the calculation of total energies. The convergence of surface energy and work of adhesion of interfaces was tested against the number of atom layers and the thickness of vacuum layer.

The chemical bonding strength of a coating layer on a substrate can be characterized by the ideal work of adhesion ($W_{ad}$), which defines the energy required to separate an interface into two free surfaces. The ideal work of adhesion can be calculated by the following formula:

$$W_{ad} = \left(E_{coating} + E_{substrate} + E_{interface}\right)/A \tag{10}$$

where $E_{coating}$ is the total energy of the isolated coating, $E_{substrate}$ the total energy of the isolated substrate, $E_{interface}$ the total energy of the interface including both coating and substrate, and $A$ the area of the interface. High work of adhesion of an interface means high interfacial bonding strength.

The calculated work of adhesion values of the studied interfaces are summarized in Table 1. Among the four interfaces, i.e., UN(001)/ZrN(001), UN(001)/c-$ZrO_2$(001), ZrN(001)/c-$ZrO_2$(001), and ZrN(111)/t-$ZrO_2$(111), UN(001)/ZrN(001) shows the lowest work of adhesion, indicating that the adhesion of ZrN coating on UN substrate is the weakest. A (c/t)-$ZrO_2$ interlayer deposited between UN and ZrN can significantly improve the adhesion of ZrN coating on UN substrate. Meanwhile, there are two possible terminations for c-$ZrO_2$(001) layer in the UN(001)/c-$ZrO_2$(001) interface, as shown in Figure 10 (b) and (c). The calculated work of adhesion values of the UN(001)/c-$ZrO_2$(001) interface show that O-terminated c-$ZrO_2$ interlayer has much stronger adhesion on UN substrate compared to Zr-terminated interlayer. Therefore, O termination is preferred for the deposited c-$ZrO_2$ interlayer in order to increase its adhesion on UN substrate. It should be noted that c-$ZrO_2$ was adopted to simulate the adhesion of ZrO coating on UN substrate. In reality, the first few nanometers of $ZrO_2$ coating should be amorphous. However, the adhesion

10

between amorphous $ZrO_2$ and UN is expected to be even stronger than that between c-$ZrO_2$ and UN due to the reduced lattice strain. Therefore, it can be concluded that a thin $ZrO_2$ interlayer should be helpful for improving the adhesion of ZrN coating on UN substrate.
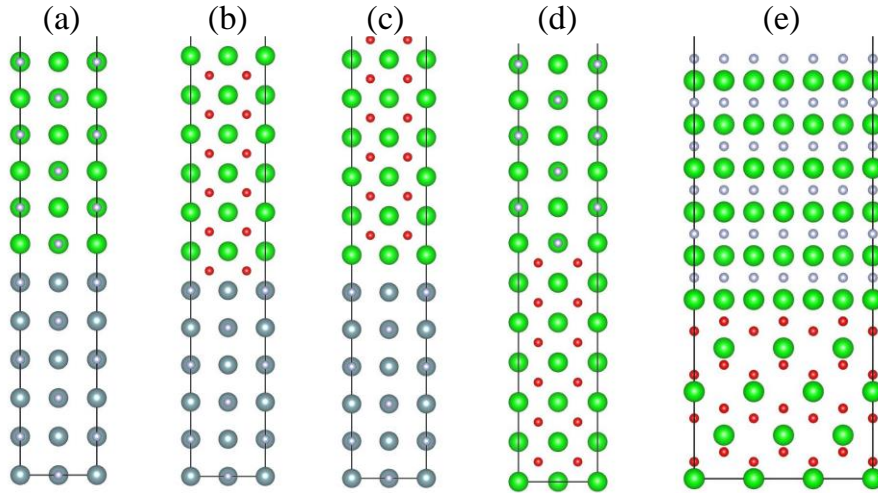


Figure 10: Interface model structures of (a) UN(001)/ZrN(001), (b) UN(001)/c-ZrO2(001)_O-term, (c) UN(001)/c-ZrO2(001)_Zr-term, (d) ZrN(001)/c-ZrO2(001), and (e) ZrN(111)/t-ZrO2(111) interfaces. Cyan, green, red and silver spheres represent U, Zr, O and N atoms, respectively.

Table 1: Calculated work of adhesion of the studied interfaces.

| Interface models | $W_d$ (J/m$^2$) |
|---|---|
| UN(001)/ZrN(001) | 1.97 |
| UN(001)/c-ZrO$_2$(001)_O-term | 4.05 |
| UN(001)/c-ZrO$_2$(001)_Zr-term | 1.49 |
| ZrN(001)/c-ZrO$_2$(001) | 5.69 |
| ZrN(111)/t-ZrO$_2$(001) | 5.76 |

## 6    FUTURE ACTIVITIES

The BISON model developed in this work provides a good basis to develop more advanced system models to explore the ALD coated particle system. Several potential areas for enhancement include:

- Creating a defected fuel kernel based on experimental results, and including convective surface conditions at boundary

11

- Adding a zirconium matrix material layer around the coating particle to explore effect of matrix region
- Adding a $ZrO_2$ interlayer between the UN kernel and ZrN coating to observe the macroscopic effects of the first principles recommendations
- Simulation of the fuel element manufacturing processes, such as mechanical rolling
- Simulation of long-term behavior under irradiation conditions
- Adding multiple particles to model to explore interactions such as contact and deformation

## 7 ACKNOWLEDGEMENT

# 8    REFERENCES

[1]     R. L. Williamson *et al.*, "BISON: A Flexible Code for Advanced Simulation of the Performance of Multiple Nuclear Fuel Forms," *Nucl Technol,* vol. 207, no. 7, pp. 954-980, 2021/07/03 2021, doi: 10.1080/00295450.2020.1836940.

[2]     BISON. "UNThermal." https://mooseframework.inl.gov/bison/source/materials/UNThermal.html (accessed 9/2/2021.

[3]     S. B. Ross, M. S. El-Genk, and R. B. Matthews, "Thermal conductivity correlation for uranium nitride fuel between 10 and 1923 K," *J Nucl Mater,* vol. 151, no. 3, pp. 318-326, 1988/02/01/ 1988, doi: https://doi.org/10.1016/0022-3115(88)90026-8.

[4]     A. A. Bauer, "Nitride Fuels: Properties and Potentials," *REACTOR TECHNOLOGY,* vol. 15, no. 2, 1972.

[5]     BISON. "UNThermalExpansionEigenstrain." https://mooseframework.inl.gov/bison/source/materials/tensor_mechanics/UNThermalExpansionEigenstrain.html (accessed 9/2/2021.

[6]     NASAGRC, "Nuclear Thermal Propulsion Materials Data Property Book Revision 2," National Aeronautics and Space Administration Glenn Research Center, Cleveland, Ohio, 2019.

[7]     BISON. "UNElasticityTensor." https://mooseframework.inl.gov/bison/source/materials/tensor_mechanics/UNElasticityTensor.html (accessed 9/2/2021.

[8]     MOOSE. "Density." https://mooseframework.inl.gov/source/materials/Density.html (accessed 9/2/2021.

[9]     S. L. Hayes, J. K. Thomas, and K. L. Peddicord, "Material property correlations for uranium mononitride: I. Physical properties," *J Nucl Mater,* vol. 171, no. 2, pp. 262-270, 1990/05/01/ 1990, doi: https://doi.org/10.1016/0022-3115(90)90374-V.

[10]    MOOSE. "HeatConductionMaterial." https://mooseframework.inl.gov/source/materials/HeatConductionMaterial.html (accessed 9/2/2021.

[11]    J.-H. Kim, G. Y. Jeong, S. Kim, Y. J. Jeong, and D.-S. Sohn, "Effect of coating thickness and annealing temperature on ZrN coating failure of U-Mo particles under heat treatment," *J Nucl Mater,* vol. 507, pp. 347-359, 2018/08/15/ 2018, doi: https://doi.org/10.1016/j.jnucmat.2018.05.019.

[12]    A. Ciriello *et al.*, "Thermophysical characterization of ZrN and (Zr,Pu)N," *J. Alloys Compd.,* vol. 473, no. 1, pp. 265-271, 2009/04/03/ 2009, doi: https://doi.org/10.1016/j.jallcom.2008.05.077.

[13]    MOOSE. "ComputeThermalExpansionEigenstrain." https://mooseframework.inl.gov/source/materials/ComputeThermalExpansionEigenstrain.html (accessed 9/2/2021.

[14]    J. Menghani, K. B. Pai, and M. K. Totlani, "Corrosion and wear behaviour of ZrN thin films," *Tribol.-Mater., Surf. Interfaces,* vol. 5, no. 3, pp. 122-128, 2011/09/01 2011, doi: 10.1179/1751584X11Y.0000000013.

[15]    MOOSE. "ComputeIsotropicElasticityTensor." https://mooseframework.inl.gov/source/materials/ComputeIsotropicElasticityTensor.html (accessed 9/2/2021.

[16]    S. Bhattacharya *et al.*, "Improving stability of ALD ZrN thin film coatings over U-Mo dispersion fuel," *Appl. Surf. Sci.,* vol. 533, p. 147378, 2020/12/15/ 2020, doi: https://doi.org/10.1016/j.apsusc.2020.147378.

[17]     W. Weinreich *et al.*, "Structural properties of as deposited and annealed ZrO2 influenced by atomic layer deposition, substrate, and doping," *J. Vac. Sci. Technol., A,* vol. 31, no. 1, p. 01A119, 2013, doi: 10.1116/1.4765047.

[18]     G. Kresse and J. Furthmüller, "Efficient iterative schemes for ab initio total-energy calculations using a plane-wave basis set," *Phys. Rev. B,* vol. 54, no. 16, p. 11169, 1996. [Online]. Available: http://link.aps.org/abstract/PRB/v54/p11169.

[19]     G. Kresse and D. Joubert, "From ultrasoft pseudopotentials to the projector augmented-wave method," *Phys. Rev. B,* vol. 59, no. 3, p. 1758, 1999. [Online]. Available: http://link.aps.org/abstract/PRB/v59/p1758.

[20]     P. E. Blöchl, "Projector augmented-wave method," *Physical Review B,* vol. 50, no. 24, p. 17953, 1994. [Online]. Available: http://link.aps.org/abstract/PRB/v50/p17953.

[21]     J. P. Perdew, K. Burke, and M. Ernzerhof, "Generalized Gradient Approximation Made Simple," *Phys. Rev. Lett.,* vol. 77, no. 18, p. 3865, 1996. [Online]. Available: http://link.aps.org/abstract/PRL/v77/p3865.

**Chemical and Fuel Cycle Technologies Division**
Argonne National Laboratory
9700 South Cass Avenue, Bldg. 205
Argonne, IL 60439

www.anl.gov